Journal of Materials Chemistry C

ROYAL SOCIETY OF CHEMISTRY

PAPER

View Article Online
View Journal

Cite this: DOI: 10.1039/d6tc00270f

Horizontally oriented pyrido[2,3-*b*]pyrazine-based thermally activated delayed fluorescence emitters exhibiting bipolar charge transport for efficient organic light-emitting diodes

Domantas Lekavicius, Rasa Keruckiene,* Matas Guzauskas, Dmytro Volyniuk and Juozas V. Grazulevicius*

Received 27th January 2026,
Accepted 24th March 2026

DOI: 10.1039/d6tc00270f

rsc.li/materials-c

Four pyrido[2,3-*b*]pyrazine-based donor–acceptor emitters containing carbazole or phenothiazine donor moieties are synthesized *via* a cyclization reaction followed by Buchwald–Hartwig cross-coupling. The solid-state films containing developed compounds emit conformer-assisted blue-to-red light with photoluminescence quantum yields of up to 82%. Their thermally activated delayed fluorescence (TADF) properties suggest efficient triplet-to-singlet reverse intersystem crossing under electrical excitation. Their applicability in organic light emitting diodes (OLEDs) are also enhanced by bipolar charge transport with hole mobilities in the range from 2.5×10^{-6} to 3.8×10^{-4} cm^2 V^{-1} s^{-1} and electron mobilities in the range from 1.4×10^{-6} to 4.6×10^{-5} cm^2 V^{-1} s^{-1} at electric field of 1×10^6 V cm^{-1}. Hole and electron injections into the light-emitting layers are ensured by ionisation energies of 5.26–5.55 eV and electron affinities of 2.64–2.91 eV, as determined by photoelectron emission spectroscopy. The compounds demonstrate the required tendency towards horizontal molecular orientation in thin films (horizontal orientation order parameter of up to 0.90), thereby enhancing internal light outcoupling efficiency. OLEDs with the developed compounds exhibit high internal quantum efficiency of up to 82% and external quantum efficiency of up to 21.3%.

Introduction

Since the first viable electroluminescent device was reported by Tang and Van Slyke,[1] one of the hurdles faced in research is efficiency. In OLEDs, electrically injected charge carriers recombine to form singlet and triplet excitons in a 1 : 3 ratio.[2] Therefore, this property of organic semiconductors significantly influences both the internal (η_{int}/IQE) and external (η_{ext}/EQE) quantum efficiencies of OLEDs, as predicted by the following formula.[3]

$$\eta_{ext} = \eta_{int} \times \eta_{out} = \gamma \times \varphi_{PL} \times \eta_{out} \quad (1)$$

According to the formula, organic light-emitting semiconductors are expected to demonstrate an optimal combination of charge-transporting properties, with the charge-balance factor (γ) approaching unity. This factor is most likely achieved when organic light-emitting layers contain either a host(s) or emitter(s) with balanced hole and electron mobilities and appropriate energy levels for hole and electron injection. Additionally, they should possess singlet and triplet-harvesting capabilities that enable exciton production efficiency (χ) near to unity, emit with a photoluminescence quantum yield (ϕ_{PL}) close to unity, and achieve improved outcoupling efficiency (η_{out}) through the utilization of horizontally oriented emitter molecules.[4] Exploiting fluorescence from emissive harvesting singlets only of organic emitters limits the maximum η_{int} of OLEDs to 25%. One of the ways to collect the remaining 75% of triplet excitons and reach χ of unity, allowing a theoretical η_{int} of 100%, is thermally activated delayed fluorescence (TADF).[5] Purely organic TADF emitters have been widely developed in the past decade primarily for use in OLEDs. Exciton dynamics, including the triplet-to-singlet upconversion through reverse intersystem crossing (rISC), enables the harvesting of dark triplet excitons for high electroluminescence efficiencies of OLEDs.[6] It is also worth mentioning that the η_{out} of typical OLEDs is significantly limited by the low light outcoupling efficiency resulting from the total internal reflection at the interfaces of optically distinctive layers.[7] This can be alleviated through the introduction of light outcoupling strategies, such as external microlens arrays, internal scattering or nanostructured layers and the control of molecular orientation. All these activities allow to effectively reduce optical trapping and enhance the external quantum efficiency.[8,9] The search for organic semiconductors that possess the ideal combination of charge-transporting ($\gamma \sim 1$), exciton-harvesting ($\chi \sim 1$), light-emitting

Department of Polymer Chemistry and Technology, Kaunas University of Technology, K. Barsausko St. 59, LT-50254, Kaunas, Lithuania. E-mail: rasa.keruckiene@ktu.lt, juozas.grazulevicius@ktu.lt

($\phi_{PL} \sim 1$), and internal light outcoupling ($\eta_{out} > 0.25$) properties is vitally required for the development of efficient OLEDs.

Pyrido[2,3-*b*]pyrazine acceptor is known for its high electron-accepting ability, due to its additional pyridine N-atoms in the fused ring mimicking quinoxaline.[10] Hence, its derivatives are used for the fabrication of electroluminescent devices. Recently, derivatives of pyrido[2,3-*b*]pyrazine attracted growing interest due to their easily tuneable full-spectrum emission *via* attachment of the different donor fragments, straightforward synthesis, and potential as TADF emitters.[11,12] Huang *et al.* reported on two 10-dimethylacridine (DMAC) or 10*H*-phenoxazine (PXZ) fragments containing pyrido[2,3-*b*]pyrazine (PP)-based emitters (**PP-DMAC** and **PP-PXZ**) exhibiting green and orange TADF respectively. The thin films of **PP-DMAC** showed a promising photoluminescence quantum yield (PLQY) of 83% while PLQY of the films of **PP-PXZ** reached 31%. OLEDs based on both compounds showed relatively high EQE values of 14.1 and 13%, respectively, as well as an improved EQE roll-off when compared to their quinoxaline-based analogues.[11] Yu *et al.* reported on a family of six pyrido[2,3-*b*]pyrazine-based emitters exhibiting a wide range of emissions spanning the entire visible region from blue to red. Two of the compounds (10-(2,3-diphenylpyrido-[2,3-*b*]pyrazin-7-yl)-9,9-diphenyl-9,10-dihydroacridine and 10-(2,3-diphenylpyrido[2,3-*b*]pyrazin-7-yl)-9,9-dimethyl-9,10-dihydroacridine) exhibited yellow and orange TADF and were utilized in the fabrication of OLEDs. The resulting devices exhibited high EQE values of 20 and 15.4%, respectively, although the EQE roll-off was slightly worse than those reported previously.[12] While these studies provide valuable insight into the photophysical properties and device efficiencies of pyrido[2,3-*b*]pyrazine-based emitters, aspects such as molecular orientation and charge-transport characteristics were not addressed. The development of efficient orange-to-red TADF emitters remains a challenge. Emission in this spectral region is limited by enhanced non-radiative decay, governed by the energy gap law – where lower-energy excited states result in increased internal conversion rates and reduced PLQY.[13] Consequently, most red-emitting TADF systems have struggled to simultaneously achieve high PLQY and EQE of OLEDs.[14] Recent studies have further highlighted the intrinsic difficulty of balancing small ΔE_{ST}, sufficient oscillator strength, and efficient RISC processes in long-wavelength donor–acceptor (D–A) TADF emitters.[15] Looking at the current landscape, novel TADF emitters for various optoelectronic applications are in demand, and pyrido[2,3-*b*]pyrazine has emerged as a promising acceptor candidate. Its derivatives exhibit good performance to date, with further improvements possible by maximizing PLQY of compounds emitting in the red-orange region. The studies referenced above lack information concerning whether pyrido[2,3-*b*]pyrazines can attain the optimal combination of properties necessary for the efficient operation of OLEDs.

In this work, we aimed to provide deep insights into molecular structure–property relationships of pyrido[2,3-*b*]-pyrazine derivatives required for OLEDs. We designed and synthesised four pyrido[2,3-*b*]pyrazine derivatives containing electron-donating carbazole and phenothiazine moieties *via* a simple two-step procedure. The acceptor and donor fragments were separated *via* phenyl bridges, a known design strategy for D–A type TADF molecules that promotes spatial separation of the HOMO and LUMO, leading to a small ΔE_{ST}.[5,16] Experimental results, in combination with those of the theoretical calculations, were used to examine the emission nature of the

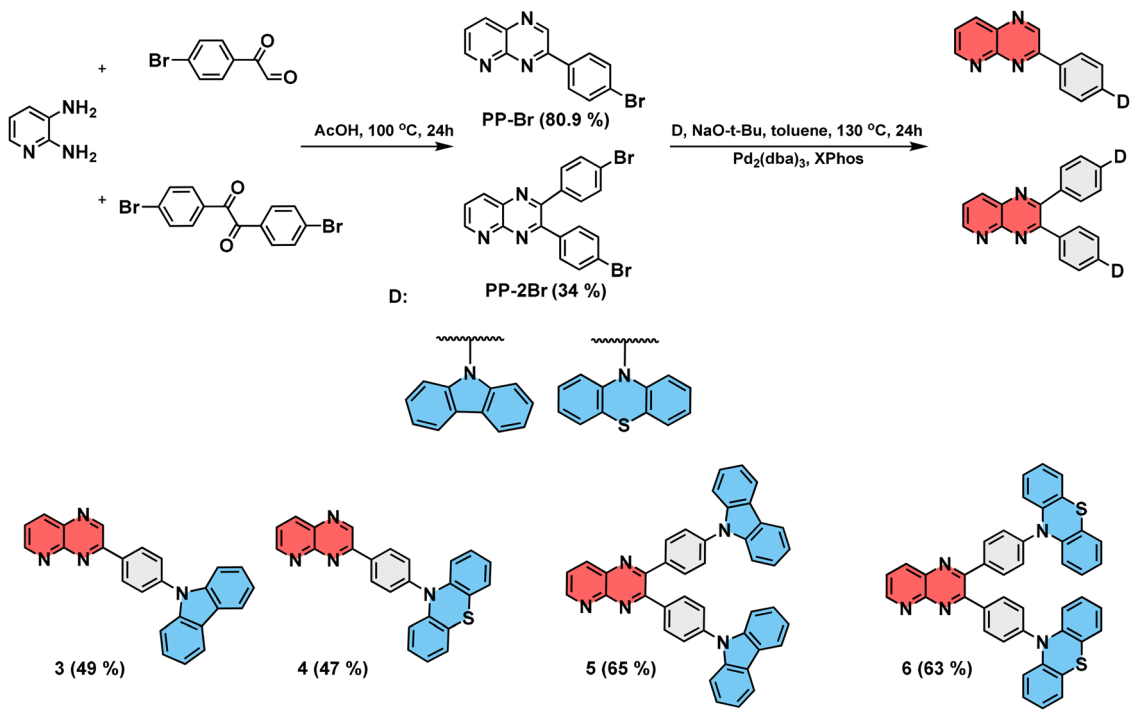

Scheme 1 Synthesis scheme of the target compounds and their structures.

compounds. It was found that the synthesized series of compounds exhibit blue to red TADF and demonstrate favourable properties for application in OLEDs. The applicability of these compounds as emitters in multilayer devices was investigated and is presented.

Results and discussion

Synthesis

The synthesis pathway for compounds **3**, **4**, **5** and **6** as well as their molecular structures are shown in Scheme 1. The first was cyclization reactions to synthesize acceptors **PP-Br** and **PP-2Br** with the yields of 80.9% and 34.0%, respectively.[11] The target compounds were then obtained by a palladium-catalysed Buchwald–Hartwig cross-coupling reactions.[17]

The structures of the target pyrido[2,3-*b*]pyrazine derivatives **3–6** were confirmed by ^{1}H, ^{13}C NMR, FTIR spectroscopies and mass spectrometry (see Fig. S1–S3). The products were found to be moderately soluble in common organic solvents. The compounds were more soluble in polar (*e.g.* ethyl acetate) and halogenated solvents (*e.g.* chloroform) than in non-polar solvents (*e.g.* hexane). The detailed synthetic procedures for the acceptors and the target compounds are provided in the SI.

Theoretical study

DFT calculations were employed to gain a deeper insight into the structure–properties relationships of pyrido[2,3-*b*]pyrazine-based compounds **3–6** (Fig. 1). The dihedral angles between the acceptor moiety and the phenyl bridge of the ground-state optimized geometries ranging from 3° to 17° degrees were estimated. The dihedral angles between phenyl bridge and donor moieties of 51° and 49° were calculated for the carbazole derivatives **3** and **5**. The dihedral angles of 85° were determined for the phenothiazine derivatives **4** and **6**.

Such not fully perpendicular geometries keep a controlled conjugation distance and prevent severe π–π stacking induced by distorted planar geometries. In addition, they enable very slight HOMO and LUMO overlap (Fig. 1) which allows to predict efficient light emission due to oscillator strength values exceeding 0.000. The calculated HOMOs and LUMOs are presented in Fig. 1. The electronic structures of pyrido[2,3-*b*]pyrazine-based compounds are quite similar. The HOMOs are situated on the electron donating carbazole and phenothiazine moieties, with a slight delocalization on the phenyl fragment. Whereas the LUMOs are situated on the acceptor pyrido[2,3-*b*]pyrazine fragments. The calculated HOMO energy values confirm the slightly stronger electron-donating character of phenothiazine moiety compared to that of carbazole moiety.

The calculations of molecular geometries at the excited states were additionally performed. It was observed that compounds do not undergo further geometrical changes in their molecular structures as the donor moieties are almost perpendicular with respect to acceptor units. The geometrical stability in the excitation process is significant for the control of energy losses and for inducing efficient intramolecular charge transfer (CT). The results of TD-DFT calculations predict that the dominant S_1 transition is CT in nature (HOMO → LUMO, see Fig. S4). The calculated energy gap between the singlet and triplet excited states (ΔE_{ST}) is less than 0.05 eV, indicating efficient rISC for all the compounds.

Thermal and morphological transitions

To fabricate OLEDs by thermal evaporation methods (*e.g.* vacuum deposition), high thermal stability of the compounds is required.[18] The thermal properties of the synthesized compounds (**3–6**) were investigated by thermogravimetric analysis (TGA) and differential scanning calorimetry (DSC). The TGA curves, presented in Fig. 2a, show that the compounds exhibit high thermal stability with 5% weight loss temperatures ($T_{D5\%}$) exceeding 300 °C. The di-substituted pyrido[2,3-*b*]pyrazine-based compounds containing two carbazole (**5**) or phenothiazine (**6**) moieties each were observed to have the highest temperatures of the onset of thermal degradation (434 °C). The full weight loss in a single stage of compound **3** shows that $T_{D5\%}$ indicates the temperature of the onset of sublimation but not of the thermal degradation.

The DSC curves of the 2nd heating scans are presented in Fig. 2b. During the 2nd heating scans, compounds **3**, **4**, **6**

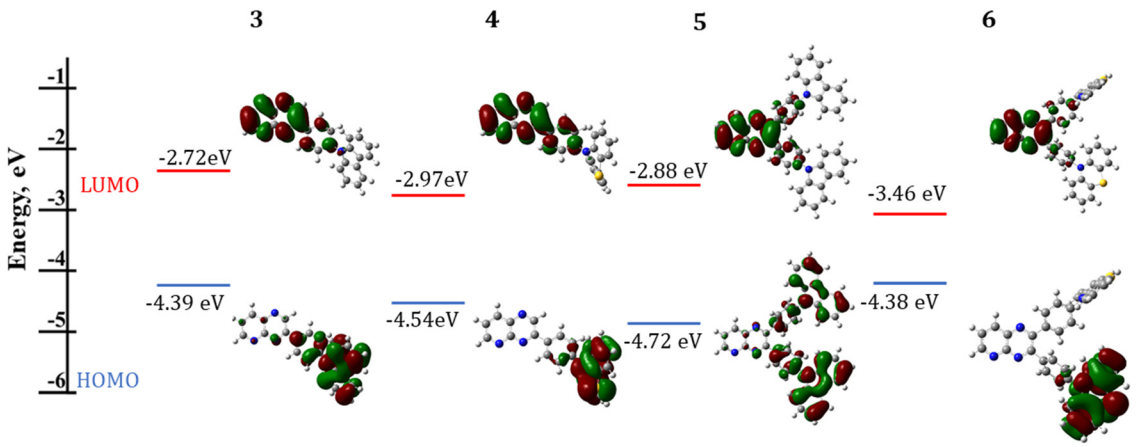

Fig. 1 Optimized frontier orbitals of pyrazine derivatives **3–6** at the ground level (calculated for vacuum).

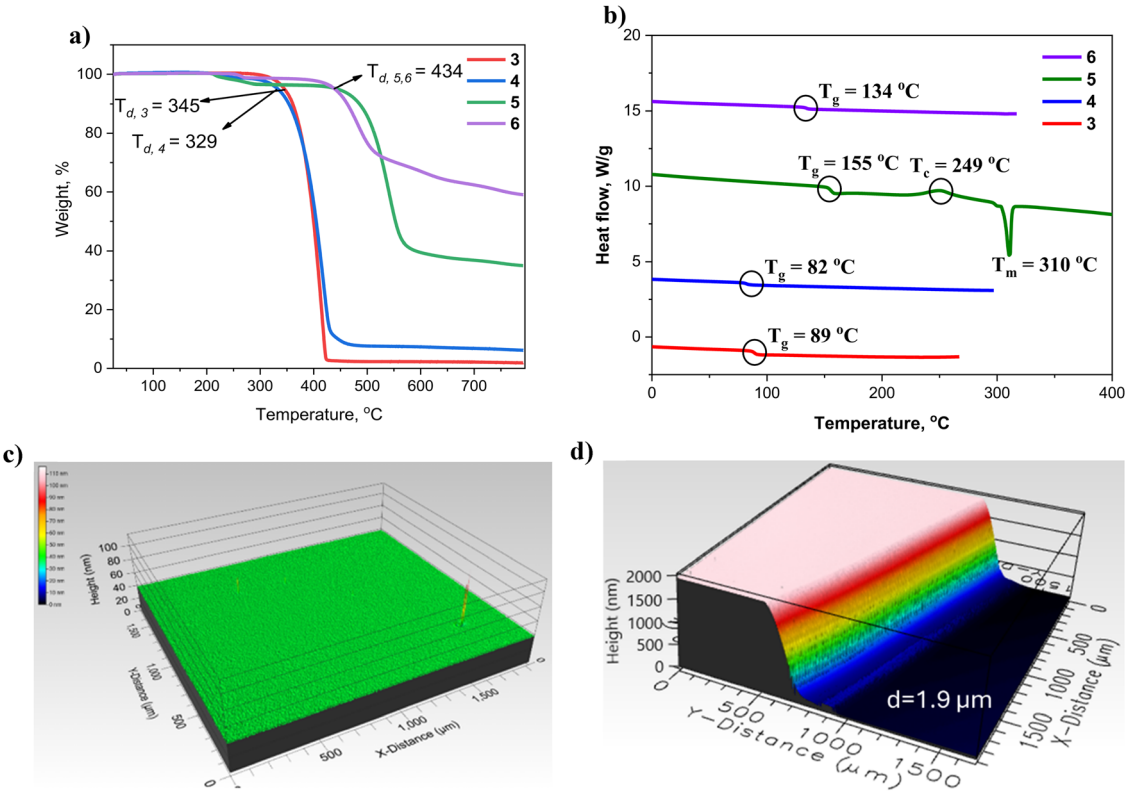

Fig. 2 TGA (a) and DSC (b) curves of the tested compounds. The pictures (c) and (d) of the surface of film of **5** was taken by an optical profilometer (Profilm3D).

exhibited glass transitions only with glass transition temperatures ranging from 82 to 155 °C, indicating the possibility of formation of the solid amorphous layers. Compound **5** exhibited glass transition (155 °C), crystallization (249 °C) as well as melting (310 °C, see Fig. 2b) during both the first and the second heating scans. No transitions were observed during the cooling scan. As glass transitions were observed for all the compounds (**3–6**) it can also be stated that they can all form molecular glass, which is a desirable property for potential application in fabrication of optoelectronic devices. The higher T_g values of compounds **5** and **6** having two donor moieties relative to those of compounds **3**, **4** can be attributed to higher molecular weights of the former compounds.

Additionally, film forming properties of pyrido[2,3-*b*]pyrazine derivatives (**3–6**) were investigated using an optical profilometer. The results are presented in Fig. S5. The average surface roughness values estimated for the samples are given in Table 1. The values obtained range from 2.55 to 0.57 nm and. They are close to the values reported for low roughness thin films (0.19 to 3.97 nm).[19] The film of compound **5** exhibited exceptionally smooth surface with the surface roughness of 0.57 nm, despite the 1.9 µm-thick film being tested (Fig. 2c and d). From the results obtained, it can be concluded that all the synthesised compounds **3–6** are thermally stable, capable of forming uniform solid amorphous layers and exhibit suitable layer formation properties for the fabrication of OLEDs.

Table 1 Thermal and morphological characteristics of the compounds and their films

Compound	$T_{D\text{-}5\%}$, °C	T_g, °C	T_c, °C	T_m, °C	Surface roughness, nm
3	345	89	—	—	1.45
4	329	82	—	—	2.55
5	434	155	249	310	0.57
6	434	134	—	—	1.01

Photophysical properties

The UV/Vis absorption and photoluminescence (PL) spectra of dilute toluene solutions (*ca.* 10^{-5} M) and thin films were recorded. The corresponding photophysical data are summarised in Table 2. The UV absorption spectra of the toluene solutions (Fig. 3a) show that the solutions of compounds with the carbazole donor fragment (**3** and **5**) absorb light up to 450 nm and those with the phenothiazine donor fragment (**4** and **6**) up to 500 nm. The different absorption spectra is also observed for the solid samples of the compounds (Fig. S6). The films of the compounds with the single donor moiety (**3**, **4**) can absorb light up to 650 nm, while the films of the compounds with two donor units (**5**, **6**) absorb up to 500 nm. The wavelengths of absorption maxima ($UV_{\lambda_{max}}$) of the compounds with similar structures (one or two donor fragments) are similar for both the solutions and the thin films. The strong higher-energy absorption bands, observed in Fig. 3a, below 300 nm (for **3** and **5**) and at around 330 nm (for **4** and **6**) can be attributed to the locally

Table 2 Photophysical characteristics

	Toluene solution			Thin film					Zeonex thin film		
Comp.	UV λ_{max}, nm	PL λ_{max}, nm	PLQY, %	UV λ_{max}, nm	PL λ_{max}, nm	τ_1, ns	τ_2, ns	PLQY, %	PL air λ_{max}, nm	PL vac. λ_{max}, nm	PLQY, %
3	292	468	4	242	510	3.52	16.30	13	468	468	41
4	335	649	3	203	658	5.79	19.67	13	553	553	—[a]
5	293	470	2	205	505	3.01	10.00	2	475	475	29
6	330	652	2	204	663	21.25	89.93	4	549	549	82

$\tau_{1,2}$ – lifetimes of the first and second decay components. [a] Could not be measured.

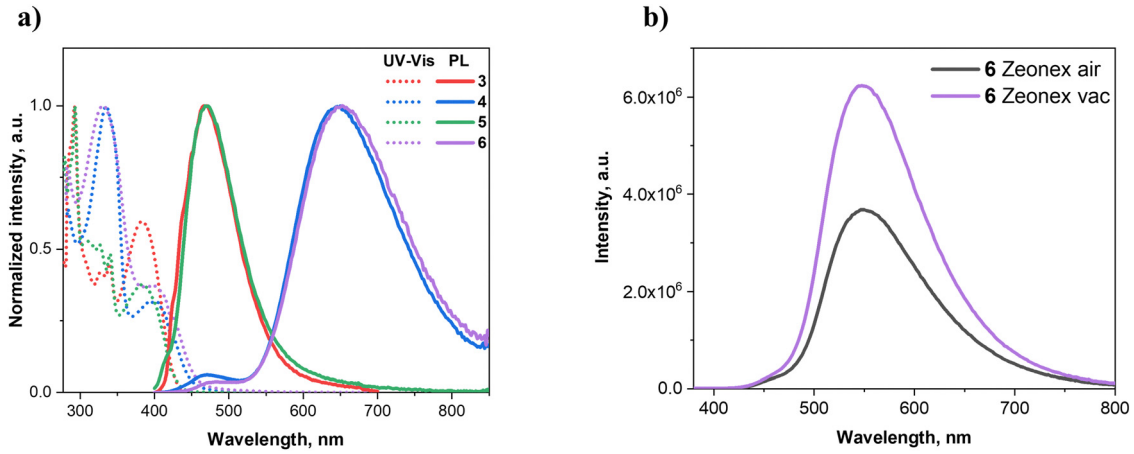

Fig. 3 Absorption and PL spectra of the toluene solutions (a); PL spectra of compound 6 dispersed in polymeric matrix Zeonex recorded in air and vacuum (b).

excited (LE) $\pi \rightarrow \pi^*$ transition of carbazole and phenothiazine moieties.[20,21] The lower-energy absorption bands above 370 nm correspond to the intermolecular charge transfer (CT) from the donor moieties to the pyrido[2,3-*b*]pyrazine acceptor moiety. In the spectra of the films (Fig. 3a), these lower-energy bands are red-shifted, appearing as a weak shoulder due to enhanced intermolecular interactions in the solid state.

The toluene solutions of the compounds exhibit blue and red emission depending on the attached donor. The incorporation of the stronger phenothiazine donor (in **4** and **6**) lead to the pronounced red shift and spectral broadening of the PL spectra in comparison to those of the solutions of the carbazole-containing analogues (**3** and **5**). The full width at half maximum (FWHM) values were estimated from the PL spectra shown in Fig. 3a. For the solutions of **3**, **4**, **5** and **6**, they were found to be of 85, 158, 81 and 163 nm, respectively. The toluene solutions of **4** and **6** exhibit dual emission, with maxima at 471 nm (LE) and 649 nm (CT) for **4**, and at 472 nm (LE) and 652 nm (CT) for **6**. The higher energy LE band is attributed to the quasi-axial conformation of the phenothiazine donor. In contrast, the lower-energy emission bands (649 nm for **4** and 652 nm for **6**) originate from the quasi-equatorial conformation with a strong CT nature.[22]

The spectra of the neat films of the compounds (Fig. S6) exhibited similar emission characteristics to those of the toluene solutions. However, the systematic red shifts of the emission bands were observed (Table 2), indicating stabilization of the emissive states in the solid environment. These shifts are more pronounced for the films of carbazole derivatives (*i.e.* emission shifted from blue to green), while the films of phenothiazine-containing compounds retained red emission with a very slight bathochromic shift. The fluorescence lifetimes (τ) of the pure thin films were estimated (Table 3) from their PL decay curves (Fig. S7). The emission decay curves of the films of the compounds were adequately described by the double exponential functions. The film of compound **6** exhibited the longest lifetime of the longer-lived component (89.93 ns). The appearance of the long-lifetime components suggests that triplet excitons are involved in the emission of the compounds, hence the compounds exhibit delayed emission.[23]

A small gap (<0.5 eV) between the singlet (E_S) and triplet (E_T) energy levels is a key factor for the manifestation of TADF.[24,25] Photoluminescence and phosphorescence spectra of the solutions of the compounds in tetrahydrofuran (THF) were recorded at 77 K (Fig. S8). The differences between the E_S and E_T values (ΔE_{ST}) were calculated. The obtained values were found to be of 0.38, 0.24, 0.38 and 0.16 eV, for compounds **3**, **4**, **5** and **6**, respectively. This observation further indicates that the emission mechanism could be TADF.

Photoluminescence (PL) spectra of the molecular dispersions (solid solutions) of the compounds in the inert rigid polymer Zeonex were recorded to determine the emission nature (Fig. 3b, S9). The emission spectra of the films of 1 wt% solid solutions of **3**, **4**, **5** and **6** in Zeonex were blue

Table 3 Energy and charge-transport parameters of compounds **3–6**

Comp.	IE_{CV}, eV	IE_{film}, eV	E_g, eV	EA_{film}, eV	μ_h, $cm^2\ V^{-1}\ s^{-1}$	μ_e, $cm^2\ V^{-1}\ s^{-1}$	β_h, $cm^{1/2}\ V^{-1/2}$	β_e, $cm^{1/2}\ V^{-1/2}$
3	5.31	5.55	2.64	2.91	1×10^{-3}	8.5×10^{-5}	10×10^{-3}	7.6×10^{-3}
4	5.43	5.25	2.51	2.74	4×10^{-6}	2.5×10^{-5}	6×10^{-3}	6×10^{-3}
5	5.54	5.54	2.71	2.83	—	1.5×10^{-5}	—	9.9×10^{-3}
6	5.45	5.26	2.62	2.64	1.5×10^{-5}	6×10^{-6}	5.2×10^{-3}	8.5×10^{-3}

IE_{CV} – ionisation energy, determined by CV, IE_{film} – ionisation energy, determined by photoelectron emission spectrometry, EA_{film} – electron affinity, $EA_{film} = IE_{film} - E_g$. μ_h and μ_e hole end electron mobilities at E of 1.3×10^6 V cm^{-1}.

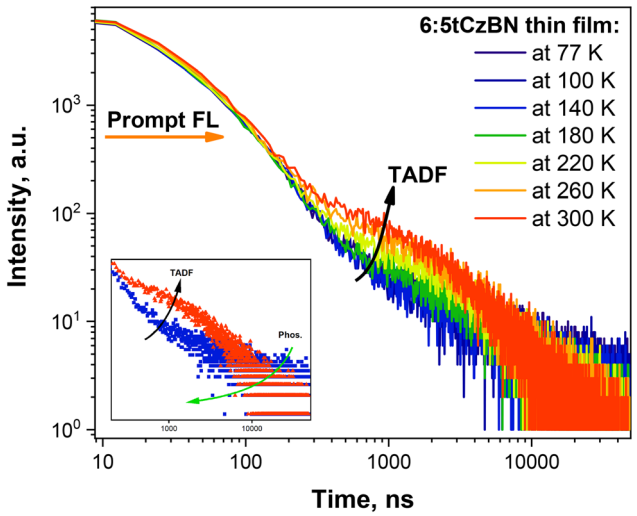

Fig. 4 Emission decay curves of the film of the solid solution of **6** in 5tCzBN recorded at the different temperatures.

shifted with respect of those of the films of the corresponding neat compounds. They exhibited blue and green emissions (Table 2). This is typically observed as Zeonex is a nonpolar polymer host.[26,27] The PLQY of compound **6** increases from 2% in toluene solution to 4% in the neat film and reaches 82% when dispersed in a Zeonex matrix (see Table 2). The moderate enhancement from solution to the neat film is attributed to aggregation-induced emission (AIE). Upon dispersion in the host, further rigidification and spatial isolation of the emissive molecules efficiently minimize intermolecular quenching, resulting in the pronounced PLQY increase. Such findings indicate, that for the compounds to be used in OLEDs, a host–guest system would be needed. The corresponding solvent polarity and aggregation-dependent photoluminescence data used to confirm AIE is provided in the SI (Fig. S10).

The emission intensities of the molecular dispersions of compounds **3–5** in Zeonex remain unchanged after evacuation. Meanwhile, the emission intensity of the molecular dispersion of compound **6** increased significantly after evacuation. The maxima of the emission spectra of the molecular dispersions of the compounds in Zeonex did not shift after evacuation.

To further confirm that the emission of phenothiazine-disubstituted pyrido[2,3-*b*]pyrazine (**6**) is TADF, it was molecularly dispersed in a host (5% in 5tCzBN) for temperature-dependent PL decay measurements. From the PL decay curves (Fig. 4), it is evident that the delayed emission component exhibits a clear temperature dependence. At low temperatures, the delayed component is suppressed and longer-lived emission attributable to phosphorescence becomes more apparent. Upon thermal activation (*i.e.* heating), the delayed emission intensifies and shortens. These observations confirm the TADF mechanism, as the efficiency of rISC is enhanced with increasing temperature.[28]

Alignment of organic light-emitting molecules

To investigate the molecular orientation of the emitters in neat films, angle-dependent photoluminescence (ADPL) measurements were performed for the thin-films (30 nm) of compounds **3–6** prepared *via* vacuum deposition. The resulting measurement curves were fitted. They are shown in Fig. 5, where they are compared to two simulated curves of isometric (0.66) and perfect horizontal (1.00) orientation.

The orientation of the molecules of compound **6** was tested both in the films of the neat compound and in those of 5% solid solutions in host 5tCzBN. However, it was determined that the introduction of the host had no effect on the horizontal orientation order parameter value (Θ_H). Therefore, the further measurements were performed using the films of the neat compounds **3–5**. The Θ_H values for the films of **3–6** were found to be 0.87, 0.75, 0.90, and 0.81, respectively. The particularly strong horizontal orientation observed for compounds **3** and **5** can be linked to their molecular structure. The presence of carbazole, a relatively rigid and planar donor fragment, increases the overall molecular planarity and anisotropy, which in turn increases the Θ_H of the compounds considerably.[29] In comparison, compounds **4** and **6**, that contain phenothiazine, showed slightly lower Θ_H values, likely due to the donor being non-planar. In addition, di-substitution of the pyrido[2,3-*b*]pyrazine core elongates the molecular length, increasing Θ_H further, when compared to the mono-substituted products. Such behaviour is consistent with reports indicating that elongated, rigid π-conjugated systems with high anisotropic polarizability tend to adopt preferential horizontal orientation during film formation due to enhanced intermolecular π–π interactions.[30,31] Overall, all four emitters exhibit a tendency toward horizontal orientation, with compounds **3**, **5** and **6** showing particularly strong alignment of transition dipoles, while the molecules of compound **4** display slightly more isotropic distribution. Such preferential horizontal orientation is beneficial for light outcoupling and suggests that the molecular design of these compounds promotes favourable alignment for optoelectronic applications.[32]

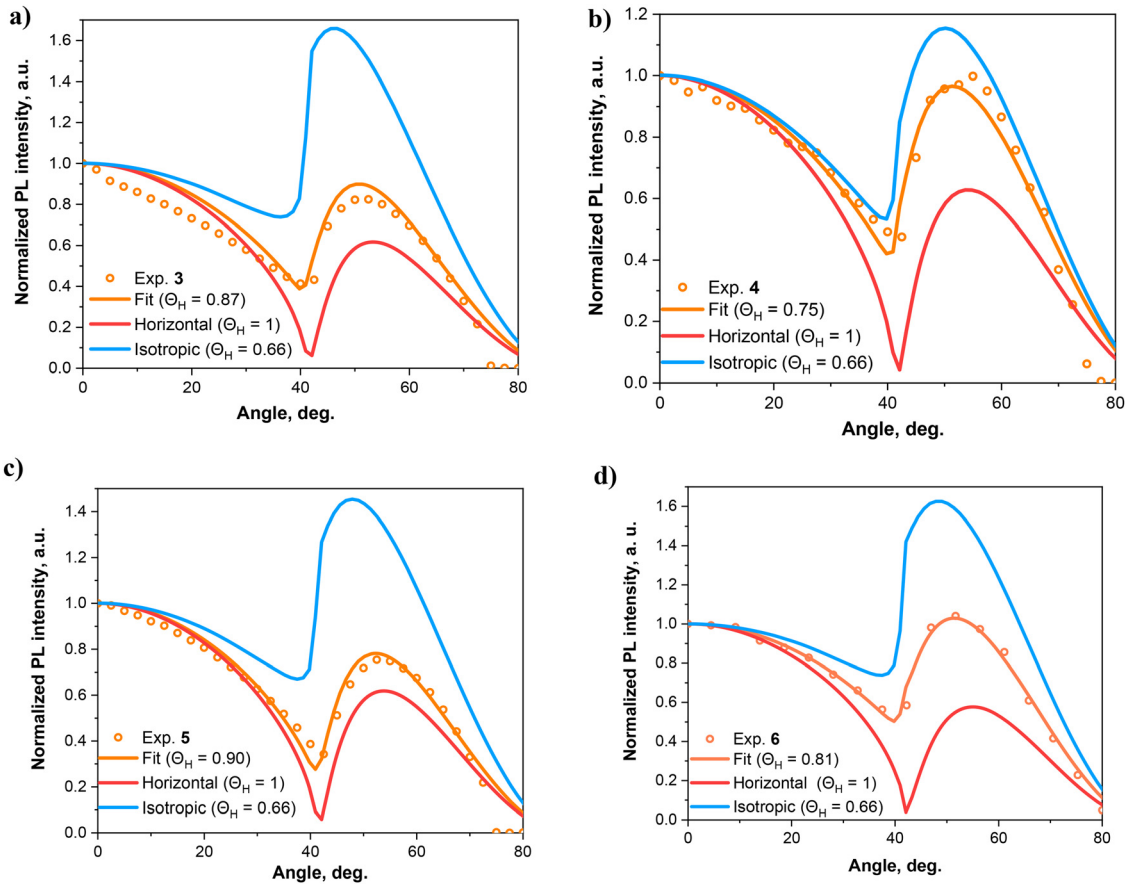

Fig. 5 ADPL intensity and simulated orientation order parameters for thin films of **3–6** (a)–(d).

Electrochemical, charge-injecting and charge-transporting properties

The electrochemical properties of the compounds were studied by cyclic voltammetry. The resulting voltammograms of compounds **3–6** are shown in Fig. S11. The values of ionisation energies (IE) of the compounds were calculated from the voltammograms. They are presented in Table 3. Compounds **3** and **4** exhibited reversible oxidations, suggesting higher electrochemical stability. Meanwhile, compounds **5** and **6** exhibited quasi-reversible oxidation up to 1.02 V.

Ionisation energies (IE_{film}) of vacuum-deposited films were determined through photoelectron emission experiments conducted in ambient air.[33,34] Photoelectron emission spectra of compounds **3–6** illustrate a distinct influence of the nature of the donor moieties (Fig. 6a). The attachment of the strong electron-donating phenothiazine moieties leads to lower ionization energies of pyrido[2,3-*b*]pyrazines **4** and **6** in comparison to IE values of pyrido[2,3-*b*]pyrazines **3** and **5**. These results indicate that holes can be injected from the anode indium tin oxide (ITO) into the layers of compounds **3–6** without intrinsic energy barriers, especially if additional hole-injecting or hole-transporting layers are included in the device structure. The similar situation holds for the electron-accepting properties (electron affinity – EA) of compounds **3–6**, given the similarity between the electron affinities of the films and the work function (2.9 eV) of the cathode LiF/Al of the established OLEDs.

It should be noted that the injected positive and negative charge carriers can cross the films of the compounds under high external electric fields, as indicated by time-of-flight (TOF) measurements (Fig. 6b, c and Fig. S12). The TOF experiment was conducted based on previous reports and can be found in SI.[35,36] The plateau and tail regions of the current transient curves for the sample of compound **3** are marked by extrapolated lines (Fig. 6b and c). The crossing points of the extrapolated lines corresponded to transit time (t_{tr}) values at different electric fields (E). The transit times were obtained from TOF current transients recorded at positive or negative voltages (V) applied to the optically transparent electrode, indium tin oxide (ITO). This observation indicates that compounds can transport both holes and electrons. All the compounds (except **5**) are capable of bipolar charge transport. The t_{tr} values were obtained from TOF current transients reconstructed on log–log scales. It was not possible to observe clear plateau and tail regions of the current transient curves plotted in linear scales for the tested samples. This is manifestation of the dispersive transport of compounds **3–6**. Hole transport was not detected for compound **5**, apparently due to the strong dispersity. Using t_{tr} values for holes or for electrons, respectively, hole

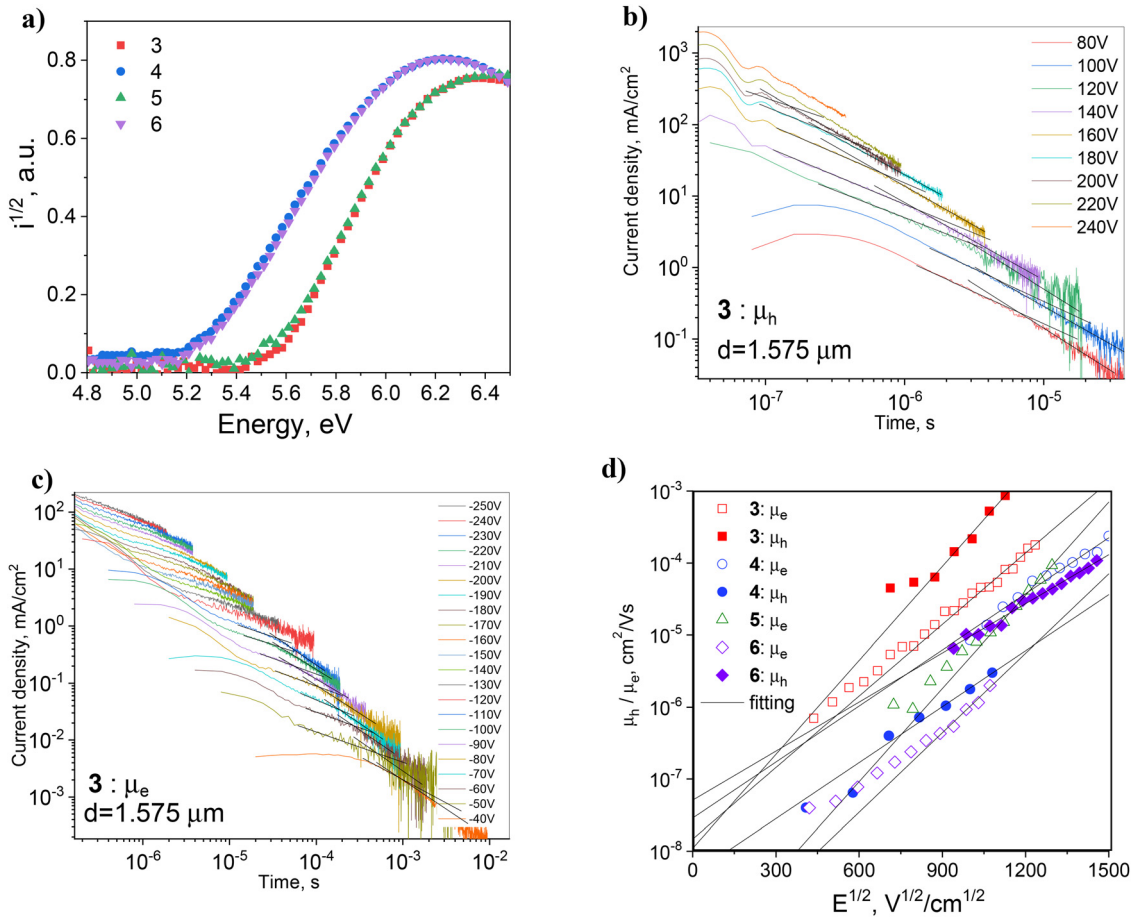

Fig. 6 Photoelectron emission spectra (a) of films of **3–6**; TOF current transients of compound **3** recorded for holes (b) at positive voltage at ITO and for electrons (c) at negative voltages at ITO. Hole and electron mobilities (d) at different electric fields are presented according to the Poole–Frenkel function for vacuum-deposited thin films of **3–6**. The lines represent the fitting results according to formula (3), while the fitting data is shown in Fig. S13.

and electron mobility values (μ_h and μ_e) were obtained at different electric fields according to the formula:

$$\mu = d^2/V \times t_{tr} \quad (2)$$

The electric-field dependence of the hole and electron mobilities was in good agreement with the following Poole–Frenkel formula, providing low fitting errors (R^2 were higher than 0.99).[37,38]

$$\mu = \mu_0 \exp \beta E^{1/2} \quad (3)$$

The formula (3) includes zero field mobility (μ_0), and the electric field dependence (β), which is related to the slopes of fitting curves. The relatively high values of β result from dispersive hole and electron transport of compounds **3–6** (Table 3). As a result, compounds exhibit high mobility only at high electric fields. Compound **5** was characterised by the highest β of *ca.* 10×10^{-3} cm$^{1/2}$ V$^{-1/2}$ for electrons. This result agrees with the prediction above that the strong dispersity prevents us from detecting hole transport in compound **5**.

The charge transporting properties of the studied pyrido[2,3-*b*]pyrazines are influenced by their molecular structures. Their hole mobilities range from 4×10^{-6} to 1×10^{-3} cm^2 V^{-1} s^{-1} and their electron mobilities range from 6×10^{-6} to 8.5×10^{-5} cm^2 V^{-1} s^{-1} at high electric field of 1.3×10^6 V cm^{-1} (Fig. 6d and Table 3). The relatively wide range of charge mobilities is attributed to the different molecular structures and to the different molecular packing in the solid films of the compounds. Compounds **3** and **4**, with linear molecular structures, exhibit higher charge mobilities than compounds **5** and **6** with the V-shape structures. The molecular packing can influence the HOMO–HOMO and LUMO–LUMO overlaps necessary for charge transport in the layers of organic semiconductors and in the host–guest layers.[39,40] The charge transporting properties of the studied pyrido[2,3-*b*]pyrazines correlate well with the results presented in the section "Alignment of organic light-emitting molecules". Most likely, the well-oriented linear molecules of compound **5** in vacuum-deposited films are the main reason for the highest hole and electron mobilities.

Electroluminescence

For the study of the relationship between the molecular properties of pyrido[2,3-*b*]pyrazine-based emitters and the electroluminescent performance of OLEDs containing these emitters,

Table 4 Electroluminescent parameters of the developed OLEDs

Device	Emitter (x wt%)	Host	λ^a, nm	CIE (x,y)	$V_{on}{}^b$, V	CE,^{c} cd A^{-1}	PE,^{c} lm W^{-1}	EQE,^{c} %
ITO/HAT-CN/TCTA/EML/TPBi/LiF/Al								
H1	**6** (2%)	5tCzBN	548	0.370, 0.507	5.5	46.1	26.6	16.3
H2	**6** (5%)		566	0.437, 0.511	6.2	48.6	28.2	18
H3	**6** (10%)		572	0.461, 0.504	6.5	46.2	22.5	17.5
H4	**6** (20%)		578	0.482, 0.496	6.7	39.3	22.4	15.5
R4	**6** (10%)	mCP	553	0.414, 0.545	6.1	49.6	34.9	16.5
ITO/PEDOT:PSS/NPB/TCTA/EML/TSPO1/TPBi/LiF/Al								
H5	**6** (10%)	5tCzBN	585	0.495, 0.481	3.1	52.5	40.2	21.3

^{a} The wavelength of electroluminescence maximum. ^{b} The turn-on voltage at the brightness of 10 cd m^{-2}. ^{c} Maximum current efficiency, power efficiency, or external quantum efficiency.

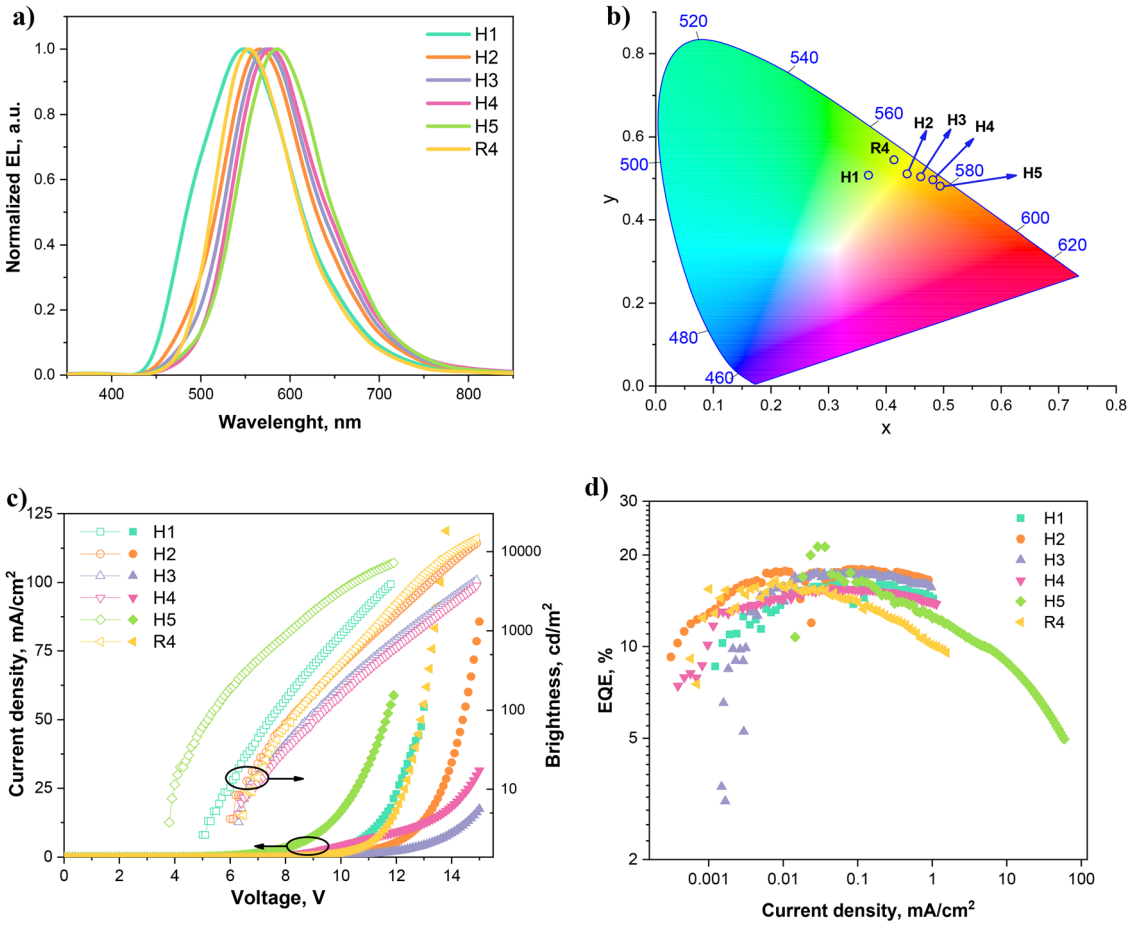

Fig. 7 Electro-optical properties of devices H1–H5 and R4. (a) EL of OLEDs; (b) CIE diagram (x, y coordinates given in Table 4); (c) plots of brightness and current density *versus* voltage (*JVL*); (d) EQE as a function of current density curves.

the device structure underwent several rounds of optimisation. The detailed process is described in further detail in the SI.

Host-containing OLEDs (H1–H4) were fabricated using the following device stack: indium-tin-oxide (ITO)/1,4,5,8,9,11-hexaazatriphenyleneheacarbonitrile (HAT-CN) [5 nm]/4,4′,4″-tris(carbazol-9-yl)triphenylamine (TCTA) [50 nm]/emissive layer (EML) [30 nm]/2,2′,2″-(1,3,5-benzinetriyl)-tris(1-phenyl-1-*H*-benzimidazole) (TPBi) [40 nm]/LiF [2 nm]/Al (Fig. S17b). For the EML, compound **6** (2, 5, 10, 20 wt%) was used with a TADF host – 5tCzBN. Here, the layer of HAT-CN acts as the hole injection layer (HIL), TCTA as the hole transporting material (HTL). TPBi served as both the electron transporting and the hole blocking material due to its very deep HOMO energy level (6.2/6.7 eV).[41] The layer of LiF acts as an electron-injection layer by modifying the work function of the aluminium cathode. Devices H1-H4 exhibited electroluminescence in the range of 548–578 nm. The progressive red shift was observed as the concentration of the emitter in the host–guest system increased

from 2 to 20% (Table 4 and Fig. 7a). The turn-on voltage of the devices ranged from 5.5 to 6.7 V at 10 cd m^{-2}. EQE ranged from 15.5 to 18%, with the current efficiency (CE) range of 39.3–48.6 cd A^{-1} and power efficiency (PE) range from 22.4 to 28.2 lm W^{-1} (Table 4). OLED H2 with the concentration of emitter **6** of 5 wt% showed the best performance with a high EQE (18%), high CE and PE values (48.6 cd A^{-1} and 28.2 lm W^{-1} respectively) as well as high luminance of 12 780 cd m^{-2}. The reference device R4, fabricated employing EML with 10 wt% of **6** in mCP, displayed comparable performance (CE of 49.6 cd A^{-1}, PE of 34.9 lm W^{-1} and an EQE of 16.5%) to those of devices H1–H4.

Using formula (1) the theoretical maximum EQE for the device based on **6** was calculated to be of 18% (assuming that the light outcoupling efficiency (η_{out}) is of 0.22). Accordingly, having the experimental results (Table 4), the η_{int}/IQE was derived as:

$$\eta_{int} = \frac{\eta_{ext}}{\eta_{out}} = \frac{0.18}{0.22} = 0.818 \ = \sim \ 82\% \qquad (4)$$

The value closely matches the measured PLQY of thin-film of the solid solution in Zeonex (ϕ_{PL} = 0.82), suggesting that γ and χ are close to unity (*i.e.* the charge-balance losses are minimal, and exciton production is highly efficient). As it is mentioned previously, the preferential horizontal orientation of the emitter is known to enhance light outcoupling. Therefore, the additional improvement of the device performance could be expected *via* further optimization.

The final optimisation was performed by replacing HAT-CN with PEDOT:PSS, introducing NPB and TSPO1. More favourable energy level alignment across the device was expected.

Structures of the molecules used in OLED H5 are shown in Fig. S16. The device H5 exhibited the notable increase in EQE (21.3%) alongside enhanced CE (52.5) and PE (40.2 lm W^{-1}), confirming the positive impact of the horizontal orientation of the emitter (see Table 4 and Fig. 7). The characteristics are better in comparison to those of the recently reported devices with pyrido[*x*,*y*-*b*]pyrazine derivatives (EQE of 12.9–20%) or quinoxaline derivatives (EQE of 15.3–18.4%) as emitters.[11,12,42,43]

Conclusions

Pyrido[2,3-*b*]pyrazine derivatives with either carbazole or phenothiazine donor moieties show high thermal stability, form molecular glasses with glass transition reaching up to 155 °C, exhibit efficient thermally activated delayed fluorescence, with photoluminescence quantum yield of the solid sample of up to 0.82. The molecules of the emitters show horizontal orientation in the neat films, achieving dipole ratios of 0.75–0.90, which benefits light outcoupling in OLEDs. The optimized OLED based on phenyl phenothiazine disubstituted pyrido[2,3-*b*]pyrazine dispersed in an appropriate host shows maximum external quantum efficiency of 21.3%. These findings indicate that pyrido[2,3-*b*]pyrazine-based molecular design with appropriately selected donor fragments is an effective strategy for the development of efficient, horizontally oriented emitters exhibiting delayed fluorescence for OLEDs.

Author contributions

Domantas Lekavicius: writing – original draft, investigation, data curation. Rasa Keruckiene: writing – review & editing, visualization, formal analysis, conceptualization. Matas Guzauskas: investigation, methodology, data curation. Dmytro Volyniuk: writing – review & editing, investigation, data curation. Juozas V. Grazulevicius: writing – review & editing, supervision, funding acquisition.

Conflicts of interest

There are no conflicts to declare.

Data availability

The data supporting this article has been included as part of the supplementary information (SI). Supplementary information is available. See DOI: https://doi.org/10.1039/d6tc00270f.

Acknowledgements

Funded by the European Union. Views and opinions expressed are however those of the author(s) only and do not necessarily reflect those of the European Union or the European Innovation Council and SMEs Executive Agency (EISMEA). Neither the European Union nor the granting authority can be held responsible for them (SCOLED, Grant Agreement No. 101098813). Dr M. Guzauskas acknowledges the support from Research Council of Lithuania (LMTLT), agreement no. S-A-UEI-23-1 (22-12-2023).

References

1 D. Sun, C. Si, T. Wang and E. Zysman-Colman, *Adv. Photonics Res.*, 2022, **3**, 2200203.
2 F. Li, A. J. Gillett, Q. Gu, J. Ding, Z. Chen, T. J. H. Hele, W. K. Myers, R. H. Friend and E. W. Evans, *Nat. Commun.*, 2022, **13**, 1–9.
3 C. Adachi, M. A. Baldo, M. E. Thompson and S. R. Forrest, *J. Appl. Phys.*, 2001, **90**, 5048–5051.
4 J. H. Lee and C. T. Chen, *J. Chin. Chem. Soc.*, 2023, **70**, 2089–2109.
5 J. Adachi and H. Okada, in *Advanced Display Technology*, ed. I. B. Kang, C. W. Han and J. K. Jeong, Springer, Singapore, 2021, pp. 39–65.
6 M. Mamada, S. Yada, M. Hayakawa, R. Uchida, H. Katagiri, T. Hatakeyama and C. Adachi, *Commun. Chem.*, 2024, **7**, 1–6.
7 J. H. Kim, J. W. Han, D. J. Lee, S. A. N. Entifar, Z. R. Ramadhan, K. T. Lim and Y. H. Kim, *Org. Electron.*, 2018, **54**, 204–208.

8 M. C. Gather and S. Reineke, *J. Photonics Energy*, 2015, **5**, 057607.
9 F. Tenopala-Carmona, O. S. Lee, E. Crovini, A. M. Neferu, C. Murawski, Y. Olivier, E. Zysman-Colman and M. C. Gather, *Adv. Mater.*, 2021, **33**, 2100677.
10 D. M. Kapse, O. S. Singh, M. Ghadiyali, S. Chacko and R. M. Kamble, *RSC Adv.*, 2022, **12**, 6888–6905.
11 T. Huang, D. Liu, J. Jiang and W. Jiang, *Chem. – Eur. J.*, 2019, **25**, 10926–10937.
12 L. Yu, Z. Wu, G. Xie, J. Luo, Y. Zou, D. Ma and C. Yang, *J. Mater. Chem. C*, 2020, **8**, 12445–12449.
13 Y. Wang, J. Ren and Z. Shuai, *Nat. Commun.*, 2023, **14**, 5056.
14 B. H. Zhang, S. Q. Liu, J. X. Pei, M. T. Luo, Y. Chen, Q. Y. Jia, Z. X. Wu and D. D. Wang, *Chem. Sci.*, 2024, **15**, 5746–5756.
15 J. Wang, Y. Niu, Y. Jiang, Z. Chen, C. Yao, W. Yao, M. He and J. Zhang, *Mater. Today Chem.*, 2025, **47**, 102796.
16 J. Wang, Y. Yang, F. Gu, X. Zhai, C. Yao, J. Zhang, C. Jiang and X. Xi, *ACS Appl. Mater. Interfaces*, 2023, **15**, 59643–59654.
17 M. M. Heravi, Z. Kheilkordi, V. Zadsirjan, M. Heydari and M. Malmir, *J. Organomet. Chem.*, 2018, **861**, 17–104.
18 S. Izumi, P. Govindharaj, A. Drewniak, P. Z. Crocomo, S. Minakata, L. E. de Sousa, P. de Silva, P. Data and Y. Takeda, *Beilstein J. Org. Chem.*, 2022, **18**, 459–468.
19 N. Kumar, T. M. Wilkinson, C. E. Packard and M. Kumar, *J. Appl. Phys.*, 2016, **119**, 225303.
20 A. Slodek, D. Zych, S. Golba, S. Zimosz, P. Gnida and E. Schab-Balcerzak, *J. Mater. Chem. C*, 2019, **7**, 5830–5840.
21 C. H. Chen, W. C. Ding, B. Y. Lin, J. J. Huang, M. Kit Leung, J. H. Lee and T. L. Chiu, *Adv. Opt. Mater.*, 2021, **9**, 2100857.
22 P. V. Prabhu, V. Darshan, I. S. Divya, M. Banerjee, S. Varughese, A. Anoop, K. N. N. Unni and J. Joseph, *Chem. Sci.*, 2026, **17**, 1002–1015.
23 J. X. Hu, S. Jiang, D. H. Zhang, T. Zhao, F. L. Lin, L. Meng, X. L. Chen and C. Z. Lu, *Adv. Sci.*, 2023, **10**, 2300808.
24 Y. Liu, C. Li, Z. Ren, S. Yan and M. R. Bryce, *Nat. Rev. Mater.*, 2018, **3**, 18020.
25 J. Eng and T. J. Penfold, *Commun. Chem.*, 2021, **4**, 91.
26 T. Matulaitis, P. L. dos Santos, Y. Tsuchiya, D. B. Cordes, A. M. Z. Slawin, C. Adachi, I. D. W. Samuel and E. Zysman-Colman, *ChemistrySelect*, 2023, **8**, e202300274.
27 S. Brebels, T. Cardeynaels, L. Jackers, S. Kuila, H. Penxten, R. J. Salthouse, A. Danos, A. P. Monkman, B. Champagne and W. Maes, *J. Mater. Chem. C*, 2024, **12**, 9255–9265.
28 P. L. Santos, J. S. Ward, P. Data, A. S. Batsanov, M. R. Bryce, F. B. Dias and A. P. Monkman, *J. Mater. Chem. C*, 2016, **4**, 3815–3824.
29 Z. Xue, G. Chen, Z. Chen, W. Luo, N. Li, Z. Huang and C. Yang, *Adv. Funct. Mater.*, 2024, **34**, 2409244.
30 D. Yokoyama, *J. Mater. Chem.*, 2011, **21**, 19187–19202.
31 T. A. Lin, T. Chatterjee, W. L. Tsai, W. K. Lee, M. J. Wu, M. Jiao, K. C. Pan, C. L. Yi, C. L. Chung, K. T. Wong and C. C. Wu, *Adv. Mater.*, 2016, **28**, 6976–6983.
32 R. Keruckiene, E. Vijaikis, C. H. Chen, B. Y. Lin, J. X. Huang, C. C. Chu, Y. C. Dzeng, C. Chen, J. H. Lee, T. L. Chiu, S. Macionis, J. Keruckas, R. Butkute and J. V. Grazulevicius, *ACS Appl. Electron. Mater.*, 2023, **5**, 1013–1023.
33 H. Monjushiro, I. Watanabe and Y. Yokoyama, *Anal. Sci.*, 1991, **7**, 543–547.
34 Y. Nakayama, S. Machida, D. Tsunami, Y. Kimura, M. Niwano, Y. Noguchi and H. Ishii, *Appl. Phys. Lett.*, 2008, **92**, 153306.
35 S. Tiwari and N. C. Greenham, *Opt. Quantum Electron.*, 2009, **41**, 69–89.
36 I. H. Campbell, D. L. Smith, C. J. Neef and J. P. Ferraris, *Appl. Phys. Lett.*, 1999, **74**, 2809–2811.
37 G. A. N. Connell, D. L. Camphausen and W. Paul, *Philos. Mag.*, 1972, **26**, 541–551.
38 S. V. Novikov, A. P. Tyutnev and L. B. Schein, *Chem. Phys.*, 2012, **403**, 68–73.
39 J. Cottaar, R. Coehoorn and P. A. Bobbert, *Phys. Rev. B:Condens. Matter Mater. Phys.*, 2012, **85**, 245205.
40 D. Ko, C. Jeong and J. Lee, *Nano Lett.*, 2025, **25**, 10840–10845.
41 T. D. Anthopoulos, J. P. J. Markham, E. B. Namdas, I. D. W. Samuel, S. C. Lo and P. L. Burn, *Appl. Phys. Lett.*, 2003, **82**, 4824–4826.
42 X. Li, Y. Chen, S. Li, A. Li, L. Tu, D. Zhang, L. Duan, Y. Xie, B. Z. Tang and Z. Li, *J. Mater. Chem. C*, 2023, **11**, 5217–5224.
43 S. Kothavale, R. K. Konidena, H. Lee, J. Y. Lee and R. Li, *Chem. Commun.*, 2025, **61**, 556–559.